PHYSICAL REVIEW LETTERS

Valley Vortex States in Sonic Crystals

Jiuyang Lu,[1] Chunyin Qiu,[1,*] Manzhu Ke,[1] and Zhengyou Liu[1,2,†]

[1]*Key Laboratory of Artificial Micro- and Nanostructures of Ministry of Education and School of Physics and Technology,*
Wuhan University, Wuhan 430072, China
[2]*Institute for Advanced Studies, Wuhan University, Wuhan 430072, China*
(Received 11 October 2015; published 29 February 2016)

Valleytronics is quickly emerging as an exciting field in fundamental and applied research. In this Letter, we study the acoustic version of valley states in sonic crystals and reveal a vortex nature of such states. In addition to the selection rules established for exciting valley polarized states, a mimicked valley Hall effect of sound is proposed further. The extraordinary chirality of valley vortex states, detectable in experiments, may open a new possibility in sound manipulations. This is appealing to scalar acoustics that lacks a spin degree of freedom inherently. In addition, the valley selection enables a handy way to create vortex matter in acoustics, in which the vortex chirality can be controlled flexibly. Potential applications can be anticipated with the exotic interaction of acoustic vortices with matter, such as to trigger the rotation of the trapped microparticles without contact.

In condensed matter physics, it is always of great interest to explore new internal quantum degrees of freedom of electrons. Recently, the discrete valley degree of freedom, also viewed as pseudospin, is attracting rapid growing attention [1–9]. Valley pseudospin, which labels the degenerate energy extrema in momentum space, has been widely observed in conventional semiconductors and trendy two-dimensional crystals (e.g., graphene and MoS_2). The intervalley scattering occurs scarcely due to the large separation in momentum, which makes the valley a good index to characterize the electron states. Like the spin in spintronics, the valley index is poentially a new carrier of information and thus, useful in modern electronic devices, leading to the concept of valleytronics [1–4]. Recently, much effort has been devoted to generate and detect the valley polarized current [10–18]. Many exciting phenomena associated with valley contrasting properties have been theoretically predicted and experimentally observed, such as valley filters [2,5,6,9] and valley Hall effects [3,4,7–9].

Because of the similarity of linear waves in periodical structures, valleylike frequency dispersions may also exist in the artificial crystals for classical waves, such as in photonic crystals and sonic crystals (SCs). In these systems, where both the coupling strength among meta-atoms and the symmetry of crystals can be flexibly tailored [19], the involved phenomena can be readily observed in their macroscopic characteristics. In fact, analog to the novel quantum phenomena associated with the conic dispersions, many intriguing wave transport properties have been demonstrated in the artificial crystals, such as *Zitterbewegung* oscillations [20,21], extremal transmissions [22–25], and extinction of coherent backscatterings [26,27]. In addition, the one-way edge modes that inherently stem from the topological property of crystal states

have also been extensively observed in the optic [28–37] and acoustic systems [38–43].

In this Letter, the concept of valley states is introduced to SCs for acoustic waves and the vortex nature of such states is revealed clearly. In addition to the usual momentum matching mechanism, an azimuthal rule for selectively exciting one of the degenerated valley states is established based on the rotational symmetry of a crystal. In contrast with atomic crystals, where the population and detection of purely polarized valley states often resort to external fields (e.g., strain [10,11], magnetic [12–15], and polarized light [16–18]), the acoustic valley states can be directly excited by external sound stimuli and detected from the field distributions inside and outside the SCs. The distinguishable valley signature (i.e., vortex chirality) brings us a new degree of freedom to manipulate sound. The excitation of acoustic valley states also enables us to produce a compact array of acoustic vortices with a controllable chirality, which is unattainable through conventional approaches based on transducer arrays. Similar to the valley electrons carrying orbital magnetic moments [3], the acoustic valley vortex states carry orbital angular momenta as well. This is particularly meaningful in the acoustic system that inherently lacks the angular momentum generated by spin polarizations. Considering the interaction with matter, in addition to the implications in fundamental studies, the vortex array created by crystal states may open up new application avenues, such as patterning and rotating microparticles without contact. Throughout this Letter, all full-wave calculations are performed by a commercial finite element software (COMSOL multiphysics).

As depicted in Fig. 1(a), the SC consists of a hexagonal array of regular triangular steel rods immersed in water [44], where the lattice constant $|\mathbf{a}_1| = |\mathbf{a}_2| = a$, the rotation
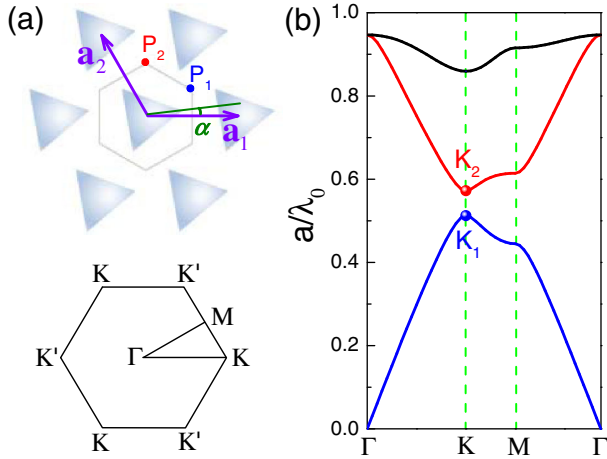
FIG. 1.   (a) Schematics of a hexagonal SC made of regular triangular steel rods immersed in water, where P_1 and P_2 indicate the positions with C_3 symmetry. Bottom panel: the corresponding FBZ. (b) The band structure of the SC with an angle $\alpha = 10°$.

FIG. 2.   Pressure field distributions for the valley states K_1 (a) and K_2 (b), where the top and bottom panels display (by color) the phase and amplitude patterns, respectively. The additional arrows in the bottom panels indicate the corresponding time-averaged Poynting vectors. Here, the sound field in the steel rods (white region) is not provided due to the weak penetration.

angle $\alpha = 10°$, and the filling ratio of rod 0.24. Figure 1(b) gives the dispersion relation of this SC along several typical directions. It displays a pair of well-defined extrema (i.e., valley states) in each corner of the first Brillouin zone (FBZ), which are separated by an *omnidirectional* band gap from the dimensionless frequency $a/\lambda_0 = 0.51$ to 0.57, with λ_0 being the wavelength in water. In contrast with the gapless graphene structure, the band gap of this SC stems from the breaking of C_{3v} symmetry (due to the mismatch of mirror symmetries between the lattice and scatterers) [19]. Below the properties of the valley states at a K point (denoted by K_1 and K_2 for the lower and higher frequency ones) are focused, and those for the inequivalent K' point can be deduced directly from the time-reversal (TR) symmetry.

Similar to electronic valley states, the acoustic valley states also exhibit exotic chirality. This can be observed from the pressure fields in Fig. 2, where the top and bottom panels display (by color) the phase and amplitude distributions, $\phi(\mathbf{r})$ and $|p(\mathbf{r})|$. In the positions of high symmetry (i.e., threefold rotational symmetry C_3), P_1 and P_2, the pressure amplitudes vanish and the phases become singular for the K_1 and K_2 states, respectively. The phase singularity can be characterized by a quantized topological charge: $n = +1$ for the K_1 state and $n = -1$ for the K_2 state. For those inequivalent states, the chirality is reversed due to the TR symmetry. The above pressure distribution reveals a typical feature of a vortex field, as shown more clearly from the arrows in the lower panels of Fig. 2, the spatial distributions of the time-averaged Poynting vectors $\langle \mathbf{S} \rangle = (2\rho_0 \omega)^{-1}|p|^2\nabla\phi$, where ρ_0 is the mass density in water and ω is the angular frequency of a sound field. As stated above, the chirality of valley vortices can be controlled by exciting the valleys of different frequencies or momenta. In fact, the vortex chirality can also be switched by rotating the orientation of the steel rods.
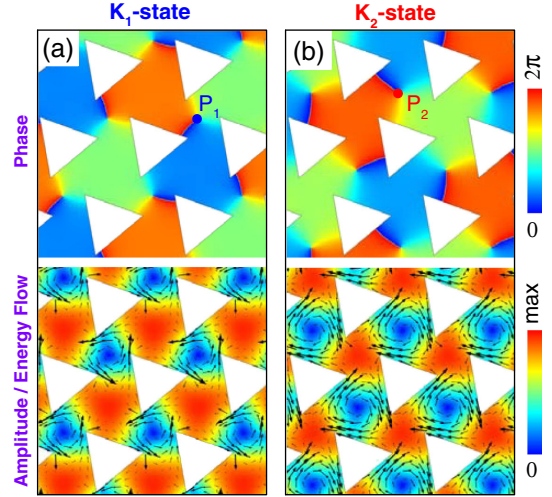
The valley states in SCs can be directly accessed by external sound stimuli. As shown in Fig. 3(a), a Gaussian beam is incident upon a regular triangle SC with a surface normal orientated along the ΓM direction, where the incident angle is chosen to satisfy the (transversal) momentum matching with the K_2 state (i.e., $k_0 \sin\theta = K/2$ with $k_0 = 2\pi/\lambda_0$ and θ being the incident angle). By this incidence, the sound field inside the SC is well excited, featured with clockwise rotated vortices (see inset, in accordance with the K_2 state). The suppression of the K_2' state can be observed more clearly in the corresponding Fourier spectrum, in contrast with the bright spots at the K points (the bright spots located on the circle stand for the input and outgoing beams traveling in free space). Note that the intervalley scattering is efficiently avoided by using the specific SC shape plus its surface orientation (ΓM direction): at each SC boundary, the K_2 state inside the SC is partly reflected back to itself and partly refracted into the free space, according to the conservation of momentum parallel to the crystal interface. Particularly, the beams leaked out (see white arrows) are experimentally detectable and in turn, serve as a good evidence of the valley selection.

The valley states can also be selectively excited by a pointlike source with proper chirality [45]. The coupling between the valley state $p_n(\mathbf{r})$ and a chiral source $p_m(\mathbf{r}) = A(r)e^{im\varphi}$ can be described by the integration $C_{n,m} = \iint p_n^* p_m d\mathbf{r}$, where n and m correspond to the topological charges of the valley state and chiral source. Under the $2\pi/3$ rotation transformation $\hat{O}$, the crystal state and the chiral source acquire extra phases, i.e., $\hat{O}p_n = p_n e^{i2n\pi/3}$ and $\hat{O}p_m = p_m e^{i2m\pi/3}$. According to the rotational invariance of the system, $\hat{O}C_{n,m} = C_{n,m}e^{i2(m-n)\pi/3} = C_{n,m}$, an
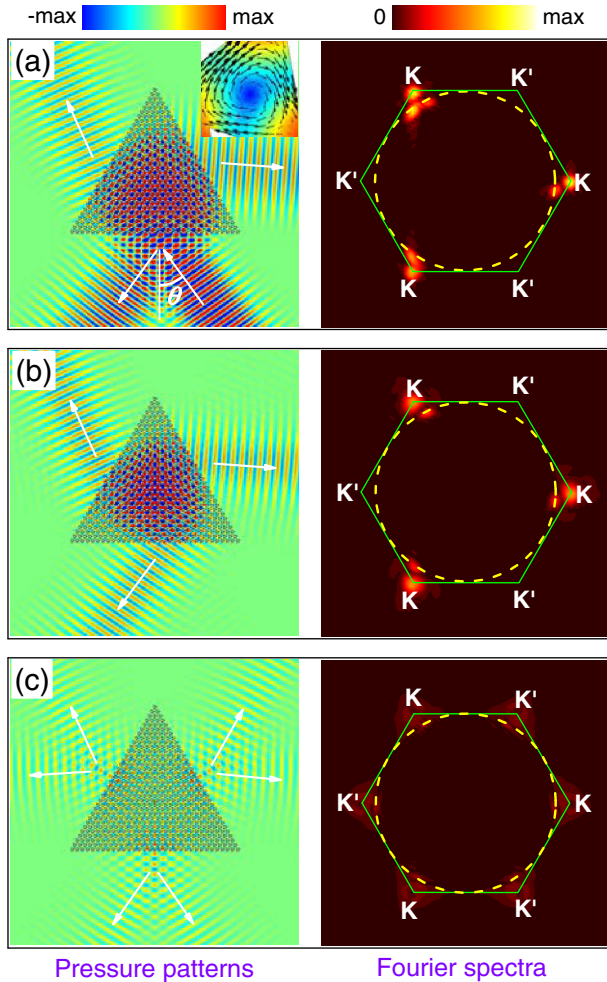
FIG. 3.   Selection rules exemplified by the K_2 state. (a) The pressure pattern generated by a Gaussian beam incident onto a finite SC obliquely, where the inset enlarges a vortex inside the SC. (b) The pressure pattern stimulated by a chiral source of topological charge $m = -1$ positioned in the center of sample (i.e., one of the equivalent P_2 points). (c) The same as (b), but for $m = 0$. All right panels display the corresponding Fourier spectra in momentum space, where the green solid and yellow dashed lines indicate the hexagonal FBZ and the isofreqency contour of free space, respectively.

azimuthal selection rule can be derived straightforwardly, i.e., $m - n = 3l$, with l being an arbitrary integer. Interestingly, a similar selection rule has been proposed in electron systems, based on the same origin of rotational crystal symmetry [4,9]. The validity of the selection rule can be demonstrated in Fig. 3(b), the pressure distribution and the corresponding Fourier spectrum stimulated by a chiral source of $m = -1$ positioned at one of the equivalent P_2 points (i.e., the locations of the vortex cores in the K_2 and K_2' states). It is observed that the K_2 state is successfully excited due to $m - n = 0$, whereas the K_2' state is completely suppressed since $m - n = -2$. For comparison, similar data for the case of $m = 0$ are provided in Fig. 3(c), which manifests that none of the valley states are excited

due to the failure of the azimuthal phase matching. The best suppression occurs exactly at the FBZ corners, despite the weak excitation of the surrounding states manifested by the faint speckles in the Fourier spectrum.

The vortex feature is not restricted in the corner states, but robustly exists in the states surrounding them. This is confirmed by the field distributions of crystal states that deviate from the valley frequencies, associated with the vortex cores that drifted away from the locations of C_3 symmetry. To characterize the quality of the vortex state, a quantity $Q = \int_{\text{Cell}} \nabla \times \langle \mathbf{S} \rangle dA$ can be defined. Physically, this quantity is proportional to the acoustic angular momentum localized in each unit cell, $J_z = \int_{\text{Cell}} \langle \mathbf{u} \times \rho_0 \dot{\mathbf{u}} \rangle_z dA$, a continuous version of the phonon's pseudospin angular momentum in atomic crystals [46,47], where $\mathbf{u}$ is the displacement of the vibration. As an example, in Fig. 4(a), we present the Q factor for the eigenstates of the second band. It is observed that the quality of the vortex state is optimized at the FBZ corners and degrades gradually toward the M point. Therefore, the vortex nature remains rather well even if the frequency deviates from the K_2 state, e.g., at the dimensionless frequency 0.60, in which the notable trigonal warping effect [48] emerges in the isofrequency contour, see Fig. 4(a). It is of interest that such a nontrivial distortion of the isofrequency contour enables a spatial separation of vortex states carrying opposite chirality, as shown in Fig. 4(b), the pressure distribution stimulated by a narrow Gaussian beam (of a width $\sim 2a$). This chirality-locked beam splitting phenomenon can be understood from the corresponding Fourier spectrum in Fig. 4(c), where the bright speckles located on the circle represent the beams traveling in free space, and the bright straight bars correspond exactly to the vortex states excited inside the SC. The excitation of the vortex states stems from the broad momentum distribution of the incident beam, and the propagating directions of the split beams can be deduced from the gradient direction of the trigonal isofrequency contour. The beam splitting behavior observed here could be viewed as a close analog to the valley Hall effect of electronic systems [3,4,7–9]. (Similar Hall effects have been extensively explored in artificial structures for electromagnetic waves [49–51].) This fascinating observation is particularly meaningful in the longitudianl wave systems without intrinsic spin polarizations, which may stimulate related experimental study of the Hall effect in acoustics.

The above study states that a great number of vortices can be generated simultaneously: the chirality could be unique in the whole SC or opposite in different spatial regions. Comparing with the conventional acoustic vortices (each made of a complex array of piezoelectric transducers or loudspeakers with carefully designed phase lags [52–54]), the vortices created by the valley states are compact and easy to fabricate. As a natural character of all chiral phased wave fields, the acoustic valley vortices carry n orbital angular
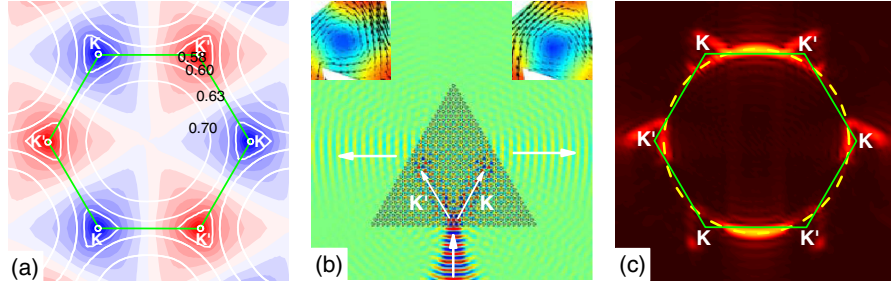
FIG. 4.   (a) The Q factor (color) of the vortex states in the second band, where blue and red indicate the clockwise and anticlockwise rotated vortices, together with several isofrequency contours (white lines) labeled in the momentum space. (b) The pressure distribution stimulated by a narrow Gaussian beam from the bottom, where the insets amplify the anticlockwise and clockwise vortices extracted from the left- and right-going beams inside the SC. (c) The Fourier spectrum of (b).

momenta and enable a wide range of applications, e.g., to induce mechnical torques on the trapped objects by transferring the angular momenta to matter.

To exhibit the capability of rotating objects by the vortex states in SCs, a dissipative rubber cylinder is placed at the vortex core and the acoustically induced torque (AIT) τ is evaluated by integrating the angular momentum density tensor over a circular contour enclosing the cylinder [55]. (Note that the probe cylinder has been verified to be well trapped in the vortex core, due to the large gradient of the field intensity.) In Fig. 5(a), we present the dimensionless AITs (scaled by the energy density integrated over a unit cell ε_{cell}) calculated for a different dissipation coefficient η of the probe cylinder [44]. It is observed that, for both the K_1 and K_2 states, the amplitudes of the AITs grow linearly with a small η and saturate gradually at a large η, associated with the signs of AITs consistent with the chirality of vortex states (thus, indicating another route to detect the chirality).
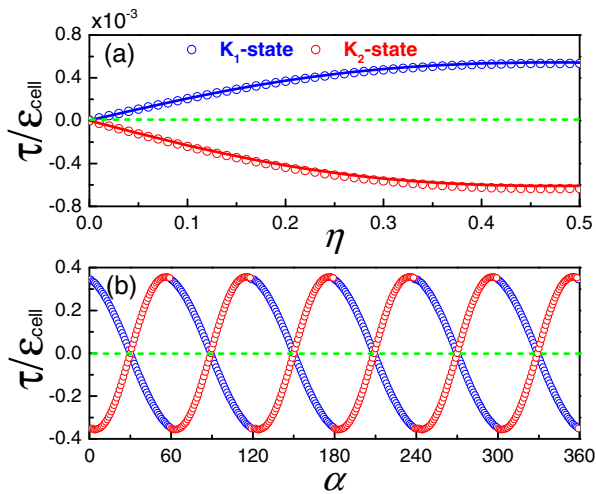

FIG. 5.   (a) The torque imposing on a rubber cylinder with a different dissipation coefficient η, where the circles are evaluated from the *anisotropic* valley vortex states, and the solid lines correspond to the theoretical predictions from the *isotropic* vortices in free space. (b) The torque perceived by the triangular steel scatterer for the SC with a different rotation angle α.

Recently, it has been theoretically proposed [56–58] and later experimentally validated [52–54] that, for an acoustic vortex in homogenous space, the AIT can be linearly connected with the power absorbed by the object, $\tau = n\omega^{-1}P_{abs}$, with n labeling again the quantized topological charge of the vortex. Does this conclusion (justified for *isotropic* vortices) still hold for *anisotropic* vortices? The question has not been addressed so far. Here, the absorptions for both valley states are evaluated and the theoretical AITs (lines) are presented in Fig. 5(a). The excellent agreement reveals that the torque-absorption relation is indeed irrelevant to the fine structure of the vortex profile. Interestingly, the exotic valley vortex states can also produce torque on the anisotropic scatterer itself. In Fig. 5(b), we present the AIT perceived by the triangular steel rod, which exhibits great sensitivity on its orientation and gives rich phenomena. In contrast with the positive slope of the K_2 state that favors the rotation of the scatterer, the negative slope of the AIT in the K_1 state tends to draw the scatterer back to its equilibrium orientation, which enables the SC to be more stable to resist undesired rotational perturbations.

In conclusion, we have extended the concept of valley states to SCs for acoustic waves. The acoustic valley states, carrying the notable feature of vortices, can be selectively accessed according to the vortex chirality. Benefited from the macroscopic nature of SCs, the valley chirality can be detected in experiments directly, which allows us a brand new manner to control sound. Similar studies can also be extended to the other artifical crystals for classical waves. In particular, the extension to vectorial wave systems, e.g., nanostructured plasmonic crystals, will enrich the inherent physics because of the additional coupling between the valley chiraly with intrinsic polorizations, leading to inspiring applications from micromoters to communications in two-dimensional integrated circuits.

*Corresponding authors.
 cyqiu@whu.edu.cn
†zyliu@whu.edu.cn

[1] X. Xu, W. Yao, D. Xiao, and T. F. Heinz, Nat. Phys. **10**, 343 (2014).

[2] A. Rycerz, J. Tworzydlo, and C. W. J. Beenakker, Nat. Phys. **3**, 172 (2007).

[3] D. Xiao, W. Yao, and Q. Niu, Phys. Rev. Lett. **99**, 236809 (2007).

[4] W. Yao, D. Xiao, and Q. Niu, Phys. Rev. B **77**, 235406 (2008).

[5] Z. Wu, F. Zhai, F. M. Peeters, H. Xu, and K. Chang, Phys. Rev. Lett. **106**, 176802 (2011).

[6] J. L. Garcia-Pomar, A. Cortija, and M. Nieto-Vesperinas, Phys. Rev. Lett. **100**, 236801 (2008).

[7] D. Xiao, G. Liu, W. Feng, X. Xu, and W. Yao, Phys. Rev. Lett. **108**, 196802 (2012).

[8] K. F. Mak, K. L. McGill, J. Park, and P. L. McEuen, Science **344**, 1489 (2014).

[9] G.-B. Liu, D. Xiao, Y. Yao, X. Xu, and W. Yao, Chem. Soc. Rev. **44**, 2643 (2015).

[10] O. Gunawan, Y. P. Shkolnikov, K. Vakili, T. Gokmen, E. P. De Poortere, and M. Shayegan, Phys. Rev. Lett. **97**, 186404 (2006).

[11] K. Takashina, Y. Ono, A. Fujiwara, Y. Takahashi, and Y. Hirayama, Phys. Rev. Lett. **96**, 236801 (2006).

[12] Y. P. Shkolnikov, E. P. De Poortere, E. Tutuc, and M. Shayegan, Phys. Rev. Lett. **89**, 226805 (2002).

[13] N. C. Bishop, M. Padmanabhan, K. Vakili, Y. P. Shkolnikov, E. P. De Poortere, and M. Shayegan, Phys. Rev. Lett. **98**, 266404 (2007).

[14] Z. Zhu, A. Collaudin, B. Fauque, W. Kang, and K. Behnia, Nat. Phys. **8**, 89 (2012).

[15] D. MacNeill, C. Heikes, K. F. Mak, Z. Anderson, A. Kormányos, V. Zólyomi, J. Park, and D. C. Ralph, Phys. Rev. Lett. **114**, 037401 (2015).

[16] K. F. Mak, K. He, J. Shan, and T. F. Heinz, Nat. Nanotechnol. **7**, 494 (2012).

[17] H. Zeng, J. Dai, W. Yao, D. Xiao, and X. Cui, Nat. Nanotechnol. **7**, 490 (2012).

[18] T. Cao *et al.*, Nat. Commun. **3**, 887 (2012).

[19] J. Lu, C. Qiu, S. Xu, Y. Ye, M. Ke, and Z. Liu, Phys. Rev. B **89**, 134302 (2014).

[20] X. Zhang, Phys. Rev. Lett. **100**, 113903 (2008).

[21] Q. Liang, Y. Yan, and J. Dong, Opt. Lett. **36**, 2513 (2011).

[22] R. A. Sepkhanov, J. Nilsson, and C. W. J. Beenakker, Phys. Rev. B **78**, 045122 (2008).

[23] X. Zhang and Z. Liu, Phys. Rev. Lett. **101**, 264303 (2008).

[24] S. R. Zandbergen and M. J. A. de Dood, Phys. Rev. Lett. **104**, 043903 (2010).

[25] S. Bittner, B. Dietz, M. Miski-Oglu, P. Oria Iriarte, A. Richter, and F. Schafer, Phys. Rev. B **82**, 014301 (2010).

[26] R. A. Sepkhanov, A. Ossipov, and C. W. J. Beenakker, Europhys. Lett. **85**, 14005 (2009).

[27] G. Weick, C. Woollacott, W. L. Barnes, O. Hess, and E. Mariani, Phys. Rev. Lett. **110**, 106801 (2013).

[28] F. D. M. Haldane and S. Raghu, Phys. Rev. Lett. **100**, 013904 (2008).

[29] Z. Wang, Y. Chong, J. D. Joannopoulos, and M. Soljačić, Phys. Rev. Lett. **100**, 013905 (2008).

[30] Z. Wang, Y. Chong, J. D. Joannopoulos, and M. Soljačić, Nature (London) **461**, 772 (2009).

[31] Y. Poo, R. Wu, Z. Lin, Y. Yang, and C. T. Chan, Phys. Rev. Lett. **106**, 093903 (2011).

[32] M. C. Rechtsman, J. M. Zeuner, Y. Plotnik, Y. Lumer, D. Podolsky, F. Dreisow, S. Nolte, M. Segev, and A. Szameit, Nature (London) **496**, 196 (2013).

[33] A. B. Khanikaev, S. Hossein Mousavi, W.-K. Tse, M. Kargarian, A. H. MacDonald, and G. Shvets, Nat. Mater. **12**, 233 (2013).

[34] W. Chen, S.-J. Jiang, X.-D. Chen, B. Zhu, L. Zhou, J.-W. Dong, and C. T. Chan, Nat. Commun. **5**, 5782 (2014).

[35] L. Lu, J. D. Joannopoulos, and M. Soljačić, Nat. Photonics **8**, 821 (2014).

[36] T. Ma, A. B. Khanikaev, S. H. Mousavi, and G. Shvets, Phys. Rev. Lett. **114**, 127401 (2015).

[37] L. Wu and X. Hu, Phys. Rev. Lett. **114**, 223901 (2015).

[38] X. Ni, C. He, X.-C. Sun, X.-p. Liu, M.-H. Lu, L. Feng, and Y.-F. Chen, New J. Phys. **17**, 053016 (2015).

[39] Z. Yang, F. Gao, X. Shi, X. Lin, Z. Gao, Y. Chong, and B. Zhang, Phys. Rev. Lett. **114**, 114301 (2015).

[40] P. Wang, L. Lu, and K. Bertoldi, Phys. Rev. Lett. **115**, 104302 (2015).

[41] M. Xiao, G. Ma, Z. Yang, Z. Q. Zhang, and C. T. Chan, Nat. Phys. **11**, 240 (2015).

[42] M. Xiao, W. Chen, W. He, and C. T. Chan, Nat. Phys. **11**, 920 (2015).

[43] V. Peano, C. Brendel, M. Schmidt, and F. Marquardt, Phys. Rev. X **5**, 031011 (2015).

[44] Material parameters: $\rho = 1.0$ g/cm^3 and $c_l = 1.49$ km/s for water; $\rho = 7.67$ g/cm^3, $c_l = 6.01$ km/s and $c_t = 3.23$ km/s for steel; $\rho = 1.2$ g/cm^3, $c_l = 2.3$ km/s and $c_t = 0.94$ km/s for rubber. Here, ρ, c_l, and c_t represent the density, longitudinal velocity, and transverse velocity, respectively. The absorption in rubber is introduced by an imaginary part of the longitudinal velocity ηc_l.

[45] Practically, the point-like chiral source can be realized by a subwavelength circular array of identical point-sources with proper phase lags.

[46] L. Zhang and Q. Niu, Phys. Rev. Lett. **112**, 085503 (2014).

[47] L. Zhang and Q. Niu, Phys. Rev. Lett. **115**, 115502 (2015).

[48] J. L. Garcia-Pomar, A. Cortijo, and M. Nieto-Vesperinas, Phys. Rev. Lett. **100**, 236801 (2008).

[49] M. Onoda, S. Murakami, and N. Nagaosa, Phys. Rev. Lett. **93**, 083901 (2004).

[50] Q. Guo, W. Gao, J. Chen, Y. Liu, and S. Zhang, Phys. Rev. Lett. **115**, 067402 (2015).

[51] A. A. High, R. C. Devlin, A. Dibos, M. Polking, D. S. Wild, J. Perczel, N. P. de Leon, M. D. Lukin, and H. Park, Nature (London) **522**, 192 (2015).

[52] K. Volke-Sepulveda, A. O. Santillan, and R. R. Boullosa, Phys. Rev. Lett. **100**, 024302 (2008).

[53] C. E. M. Demore, Z. Y. Yang, A. Volovick, S. Cochran, M. P. MacDonald, and G. C. Spalding, Phys. Rev. Lett. **108**, 194301 (2012).

[54] A. Anhauser, R. Wunenburger, and E. Brasselet, Phys. Rev. Lett. **109**, 034301 (2012).

[55] Here, the calculation is carried out from the eigenstate. The radius of the rubber cylinder is 0.1 a, which is small enough and leads to a negligible influence on the eigenstate. The

result has also been checked in a finite SC by an external excitation, which exhibits a weak dependence on the location of the vortex core because that once the valley state is excited, the vortex pattern in each lattice site keeps almost invariant except for the amplitude.

[56] J. Lekner, J. Acoust. Soc. Am. **120**, 3475 (2006).
[57] K. D. Skeldon, C. Wilson, M. Edgar, and M. J. Padgett, New J. Phys. **10**, 013018 (2008).
[58] L. K. Zhang and P. L. Marston, Phys. Rev. E **84**, 065601 (2011).